Soft Matter

Accepted Manuscript

ROYAL SOCIETY OF CHEMISTRY

www.rsc.org/softmatter

Journal Name

ARTICLE

Influence of Side Chains on the Self-alignment Capability of Electroluminescent Polyfluorenes

Received 00th January 20xx,
Accepted 00th January 20xx

DOI: 10.1039/x0xx00000x

www.rsc.org/

Sunyoung Lee, [a] Yooseong Yang, [b] Sunchul Kwon *[c] and Youngsuk Jung *[d]

We report a significant role of side chains in the propagation of molecular orientation upon annealing the liquid crystal phase of polyfluorenes. Direct rubbing of poly(9,9-di(octyl)fluorene) led to the orientation of polymer segments in the top-most region of the film and enhanced propagation of this orientation along the rubbing direction was observed upon annealing. In contrast, the rubbing-induced molecular orientation of poly(9,9-di(ethylhexyl)fluorene) segments completely disappeared upon annealing in the nematic melt state. The higher order of the side chain structures in poly(9,9-di(octyl)fluorene) were found to allow the propagation of the three-dimensional molecular alignment. From integrated experimental and density functional theory studies, we propose that side chain interdigitation generates the unique alignment behavior of poly(9,9-di(octyl)fluorene).

Introduction

Solution processes have been commonly used for the fabrication of organic semiconducting polymers with side chains for electronic applications such as photovoltaic cells,[1] organic field effect transistors,[2] and organic light-emitting-diodes (OLEDs).[3] The chemical structure of the side chains influences the three-dimensional (3D) structure of the polymers,[4–6] which can control their electronic properties.[7,8] Among organic semiconducting polymers, the commercially available poly(dialkylfluorene)s (PFs) are very promising owing to their high performance as blue LEDs[9–11] (i.e., efficient light-emitting properties,[12–14] high quantum yield,[15] and high mobility[12,16]). In the PF structure, facile substitution at the C9-position of fluorene results in good solubility in common organic solvents, which provides good processability for spin-coating or printing.[17] In addition, the rigid, planar biphenyl segments allow the formation of a thermotropic liquid crystalline mesophase, which is the transition between a partially crystalline state and a birefringent liquid state.[4,11,18–23] Such unique phase behavior is observed in the range of 100–180 °C for several PFs with alkyl substituents.[4,24] Electronic devices require component materials with anisotropic properties to obtain linear polarization or a device emitting linearly polarized light.[4,11] Consequently, the application of PFs in the field of displays has received attention because their spatially anisotropic chain structure can be aligned in their nematic melt state on an alignment layer.

To obtain a thoroughly aligned film, generally, the surface of an alignment layer such as a polyimide substrate is first rubbed with a velour cloth, and PF films on top of the alignment layer are annealed in their liquid crystalline state.[4,11,20–23] The aligned PFs, which have a high degree of molecular orientation order, enhance the anisotropic optical and electrical properties.[13,14] The alignment template in contact with the liquid crystalline layers can be combined into a single layer.[25–27] Such self-alignment using PFs would simplify the fabrication process and reduce the cost of electroluminescence devices. In principle, self-alignment with in-plane anisotropy can be achieved by rubbing or irradiation with polarized UV light. The rubbing process is commonly used because it does not influence the molecular characteristics of the film.[28] However, the effect of the rubbing process generally extends only a few nanometers below the film surface at temperatures lower than the glass transition temperature (T_g).[29,30]

Even though the well aligning features by the alignment layer, self-alignment has never been achieved for poly(9,9-di(ethylhexyl)fluorene) (PF2/6) using the rubbing process.[31,32] As the monomer units are illustrated in Fig. 1a, the branched structure of the side chains of PF2/6 are known to cause spatial limitations that prevent interdigitation. On the other hand, octyl-chains in poly(9,9-di(octyl)fluorene) (PF8) have more free space for interdigitation that induces a registry between adjacent molecules.[5,33] Herein, we investigate the influence of a direct rubbing process on the propagation of molecular orientation in PF2/6 and PF8. We carried out polarized UV-Vis absorption and optical measurements to determine the change in the in-plane molecular orientation of these PFs at annealing in their nematic melt state after surface

[a] Organic Electronic Material Lab, Samsung Advanced Institute of Technology, Suwon, Gyeonggi 16678, Korea.
[b] Energy Material Lab, Samsung Advanced Institute of Technology, Suwon, Gyeonggi 16678, Korea.
[c] Department of Civil Engineering, Pusan National University, Busan 46241, Korea. E-mail: sckwon@pusan.ac.kr
[d] Analytical Science Group, Samsung Advanced Institute of Technology, Suwon, Gyeonggi 16678, Korea. E-mail: youngs.jung@samsung.com

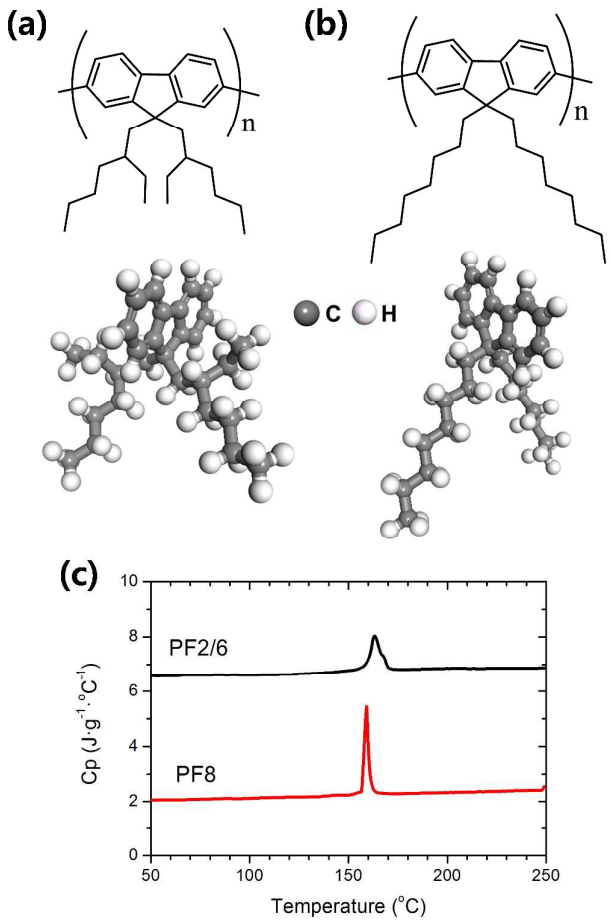

Fig. 1. Optimized geometry of the side chains of (a) di(ethylhexyl)fluorene and (b) di(octyl)fluorene using DFT calculations. (c) Endothermic thermal transitions into the nematic liquid state for PF2/6 and PF8 observed with differential scanning calorimetry (DSC). Data of PF2/6 is offset for clarity.

rubbing. In addition, we used a side chain close-packing model and density functional theory (DFT) calculations to obtain a fundamental understanding of the role of side chains in molecular orientation at the atomistic level.[34,35] We focused on understanding the configuration of interdigitation to provide a comprehensive analysis of such a molecular orientation for PF2/6 and PF8. Consequently, we propose an important synthetic design rule for side chains in PFs to obtain substantial molecular alignment.

Experimental

Thin film fabrication and rubbing process.

We used PF2/6 and PF8 with molecular weights (Mw) of 65 K and 72 K (PDI ~1.9 and ~2.0), respectively, measured by gel permeation chromatography (GPC) with polystyrene standards. The PF films were cast on tin-doped indium oxide glass substrates by spin-coating from a 5 mg/mL solution in toluene at 600(·2π) rad/min using a 60(·2π) rad/min ramp rate. The substrates were cleaned by sonication in toluene, isopropanol, and distilled water. T_g of PFs would be ~60 °C according to previous report.[36] Here the T_g was expected by extrapolation from a series of well-defined fluorene oligomers. After drying the films at 80 °C for 30 min, the film surfaces were rubbed at ambient temperature using a motorized rubbing device with a rotating velour cloth. The rubbed samples were heated for 1 h at their nematic melt temperature (~180 °C), which is well above the measured nematic transition temperature. Finally, the film was cool to 25 °C at a cooling rate of 10 °C/min. Film thicknesses of ~60 nm were measured by ellipsometry and all polymer processing was performed in a N_2 atmosphere.

Characterization of the thin films.

Nematic transition temperatures were obtained by differential scanning calorimetry (DSC) using TA Instruments DSC Q2000 with heating rate of 5 °C/min under N_2 purging. Topographical surface images of rubbed films and annealed films were scanned with an AFM (Dimension 3100, Veeco) in tapping mode. Fresh tips were used with each film and scan size of images were varied from 1 μm to 5 μm to achieve a high lateral resolution. Molecular anisotropy introduced in the films induced by rubbing or subsequent annealing was confirmed with measuring their UV-Vis absorption spectra recorded using a Perkin-Elmer Lambda 1050 UV-Vis spectrometer with a Glan-Thomson polarizer. Polarized optical microscope, Olympus BX51 microscope with polarizers, was also used to explore the anisotropy in the bulk of the films. A laboratory-scale wide-angle X-ray scattering instrument (Philips Xpert) was used for the observation of crystalline features in the films. Cu K_α radiation in conventional pinhole geometry and specular geometry for sample mounting were set. The Incidence angle of the 40 KeV/40 mA powered X-ray was fixed, and a diffraction pattern was obtained through a detector (2θ) scan.

DFT calculations.

3D chemical structures of the repeating units of PF2/6 and PF8, and subsequently, geometry optimization of two interlayers of PF2/6 and PF8 were carried out using the DMol^3 module of Materials Studio from Biovia[37] with the general gradient approximation (GGA) Perdew–Burke–Ernzerhof (PBE) functional since the GGA-PBE functional performs well in describing interactions on an organic adsorbate and various materials.[38] Here we used all-electron Kohn–Sham wave functions and the double numerical basis set with polarization (DNP). For the calculation, non-dimensional models were designed. The DFT calculations are performed at 0 K without pressure and zero-point motion. After the initial atomic positions were assigned, the geometry was optimized to refine the model structure. Once the optimized unit structures were obtained, two interlayers for each polyfluorene were

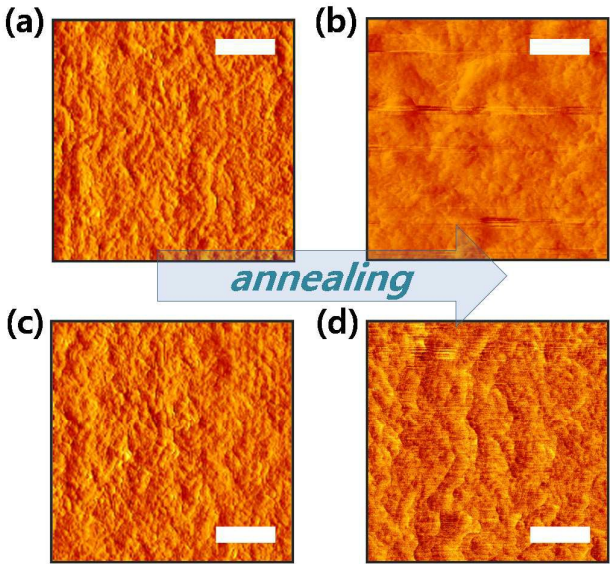

Fig. 2. AFM phase images of PF2/6 (a and b) and PF8 (c and d). (a) and (c) are the surface images of rubbed films; (b) and (d) are surfaces after annealing above the nematic phase transition temperature and then cooling. Scale bar denotes 500 nm and all images are 20 degree vertical phase scale. Rubbing directions are from bottom to top of each image.

introduced and the interlayer distances were decided by the he molecular interactions.

Results and discussion

Surface analyses.

Prior to the experimental analysis, we investigated the optimized geometry of single PF2/6 (Fig. 1a) and PF8 (Fig. 1b) units using DFT calculation to determine their molecular orientations. The side chain structures were representatively incorporated into the molecular structure of PF. The fluorene rings of the PFs were distorted along with the side chains with torsion angles of 90.5° and 102.5° for PF2/6 and PF8, respectively. We also found a relatively small free space between the fluorene rings and the side chains in PF2/6, which led to the smaller torsional angle.

To understand the self-alignment capability of PFs experimentally, we used PF2/6 and PF8 with comparable molecular weights (Mw) of 65 K and 72 K (PDI ~1.9 and ~2.0), respectively. In Fig. 1(c), both PF2/6 and PF8 exhibit a thermal transition into a nematic phase at ~162 and ~159 °C, respectively. Therefore, annealing at 180 °C resulted in the formation of liquid crystalline PFs, which have a structure consisting of a rigid backbone and free movement of the side chains.[4,11,32] Dried PF films were rubbed at first and the film surfaces slightly scratched and exhibited to have grooves that is typical features when a rubbing process are applied (Fig. 2a and c show surface phase images for the rubbed surfaces of PF2/6 and PF8, respectively). Subsequent annealing and then cooling of each film after entering into their liquid crystalline states, the top surface of PF2/6 appeared to be randomly reorganized (Fig. 2b). In case of the PF8, however, aligned electron density characteristics still remained after annealing at the nematic melt state (Fig. 2d). Obviously, AFM investigates only a few layers of the film surface, characterization tools that can explore whole region of the film depth are necessary.

Evaluation of molecular alignment.

To evaluate the alignment characteristics in the bulk region of the films, UV-Vis absorption spectra were recorded using a UV-Vis spectrometer with a Glan-Thomson polarizer. Upon direct rubbing of the film surface, only a few of the top-most molecular layers may be aligned along the rubbing direction,[32] which leads to the slight dichroism observed by polarized UV-Vis absorption of both PF2/6 and PF8, as shown in Fig. 3(a). On the other hand, after further heating and annealing of the rubbed films in their nematic melt states, the top surfaces of the PF2/6 and PF8 films showed different molecular alignment behavior. In Fig. 3(b), the identical polarized UV-Vis absorption spectra observed for the annealed

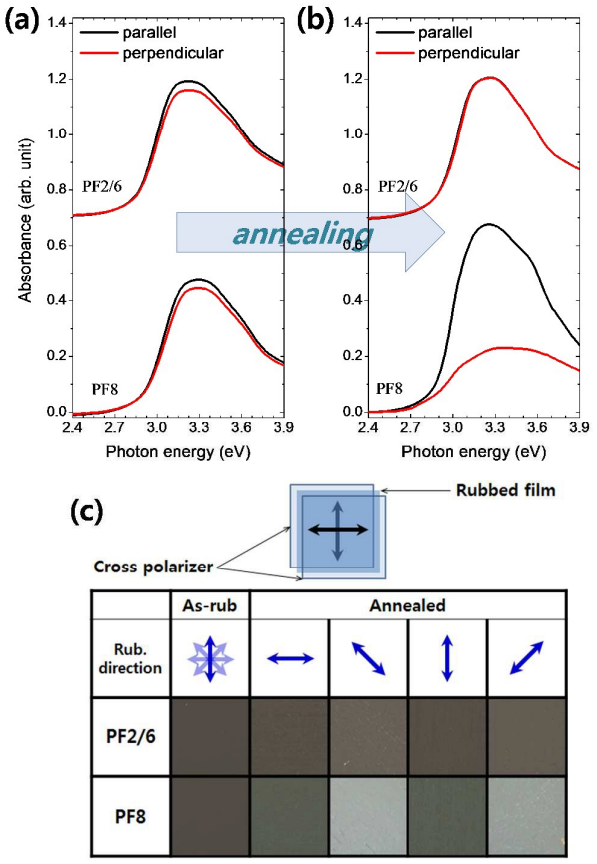

Fig. 3. Polarized UV-Vis absorption spectra for (a) rubbed PF films and (b) subsequently annealed films in the liquid crystalline state. The electric field vector of incident light was oriented in-plane parallel (black) and perpendicular (red) with respect to the rubbing direction of the film. (c) Polarized optical microscope (POM) images for the corresponding PF films. The films were located in between a cross polarizer and rotated to observe the molecular orientation, which is distinguished as brightness in the POM image according to the relative direction between the polarizer (arrows in polarizer) and the rubbing axis (arrows of Rub. direction).

PF2/6 films along the rubbing direction indicates that the rubbing-induced molecular orientation had completely disappeared, and the initial equilibrium structure was restored. Conversely, PF8 showed a substantial absorption dichroism (D ~ 3) after annealing. The higher absorption obtained for parallel polarization indicates that preferential backbone orientation was developed along the rubbing direction as the transition dipole moment in conjugated PFs is along the molecular backbone.

We evaluated the in-plane molecular anisotropy induced by the oriented top seed layers after the annealing process using polarized optical microscopy, as shown in Fig. 3c. In the samples, the birefringence of the oriented PFs provides phase contrast to the rotation of polarized light through a cross polarizer (Fig. 3c). As the film was rotated, the brightness and darkness of the image was observed at each rotational angle. PF8 provided the brightest image when the rubbing direction was angled 45° to the polarization axis. The experimental results showed that direct rubbing of the PF8 surface led to good alignment of the top-most molecular chains along the rubbing direction. Furthermore, this orientation at the film surface expanded into the bulk film, orienting the PF8 molecular chain throughout the film. This result indicates that the oriented anisotropy at the film surface is strong enough to act as an alignment template. The dichroic ratio of PF2/6 was reported to be higher than that of PF8 on an alignment layer owing to the higher molecular aspect ratio of PF2/6.[4,11] However, only PF8 showed exceptional anisotropy induced by the self-aligning configuration. It is well-known that π-stacking of conjugated fluorene rings can contribute to a 3D molecular orientation.[39] In case of PF8, it is supposed that the side chains also contribute to the reorientation of adjacent molecules. Here, the side chains between the molecules equilibrate to van der Waals radii among methylene units at the liquid crystalline phase.[40] According to the detector scanning X-ray diffraction (XRD) data shown in Figure S1 in the supporting information, there exists marked chain orientation in PF8. This could be confirmed by the peak (006) even though the degree of crystallinity for both the polymers is comparable.

Side chain interdigitation model.

Different side chain structures could result in the differences of the intermolecular configurations in the side chain region between the polymer backbones. To evaluate the differences between the two unlike side chains, we examined the intermolecular interactions and the influence of side chains between the polymer chains using a side chain close-packing model described by Kline et al.[5] If we assume the number of methylenes per unit cell area for dioctyl-branches is 2 and that for diethylhexyl-branches is ~3 (2 long side chains with 2 short side branches), the density of side chain attachment can be obtained through vector analysis, as shown in Fig. 4. In case of interdigitation, the number of methylenes per unit cell area is twice the number for non-interdigitation.[5]

If the molecular chains of PFs are interdigitated with sufficient orientational order, the side chain tilt with respect to the lamellar normal can be determined.[6] Here, the side chain tilts indicate the angle from the fluorene ring plane. It should be noted that the interdigitated side chains of PF2/6 would be denser than high density polyethylene[39] for any tilt evaluated using the π-stacking distance and distance between the side chains.[41–46] The interdigitation of PF8 side chains results in the density of polyethylene at tilts of ~20° (oval in Fig. 4) owing to the half density of octyl-branches and the interlayer distance of ~16.5 Å, as confirmed by XRD measurements. Non-interdigitated side chains of PF2/6 can have the density of polyethylene at similar tilts and could be more disordered.[47] Non-interdigitated PF8 also can exhibit the density of polyethylene, but fairly high tilts of ~60° are required (arrow in Fig. 4), which implies that the side chains of PF8 are partially interdigitated.

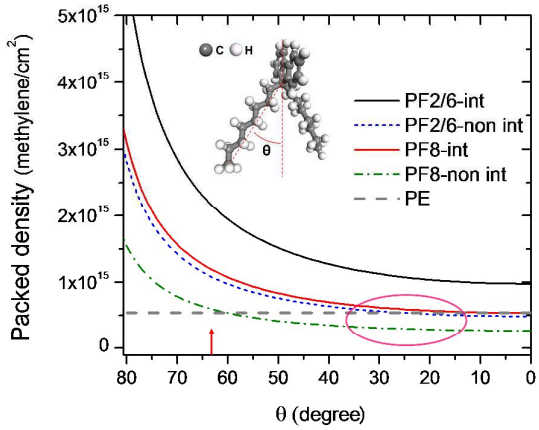

Fig. 4. Calculated packing density of PF as a function of the side chain tilt for interdigitated PF2/6, non-interdigitated PF2/6, interdigitated PF8, non-interdigitated PF8, and dense aliphatic polyethylene. The tilt angle, θ, is relative to the fluorene ring plane. Oval and arrow indicate interdigitatied and non-interdigitated side chain tilt angle of PF8, respectively, when its density is maintained to that of polyethylene.

Geometry between adjacent molecules.

To unambiguously determine the influence of side chains in PFs on the self-alignment, we carried out a geometry optimization of two interlayers of PF2/6 and PF8. This can provide a comprehensive analysis of the correlation between the interaction characteristics of the PF layers and the molecular orientation, as shown in Fig. 5. Overall, the optimized geometry of PF8 supports that the side chains could critically contribute to the 3D molecular orientation. In all cases, the interlayer interaction during interdigitation leads to a reduction in the interlayer distance. After interdigitation, the side chains of the PFs likely fill the space between lamellae;[5,41,42] however, in PF8, the upper layer is clearly interdigitated with the lower layer, as compared with PF2/6.

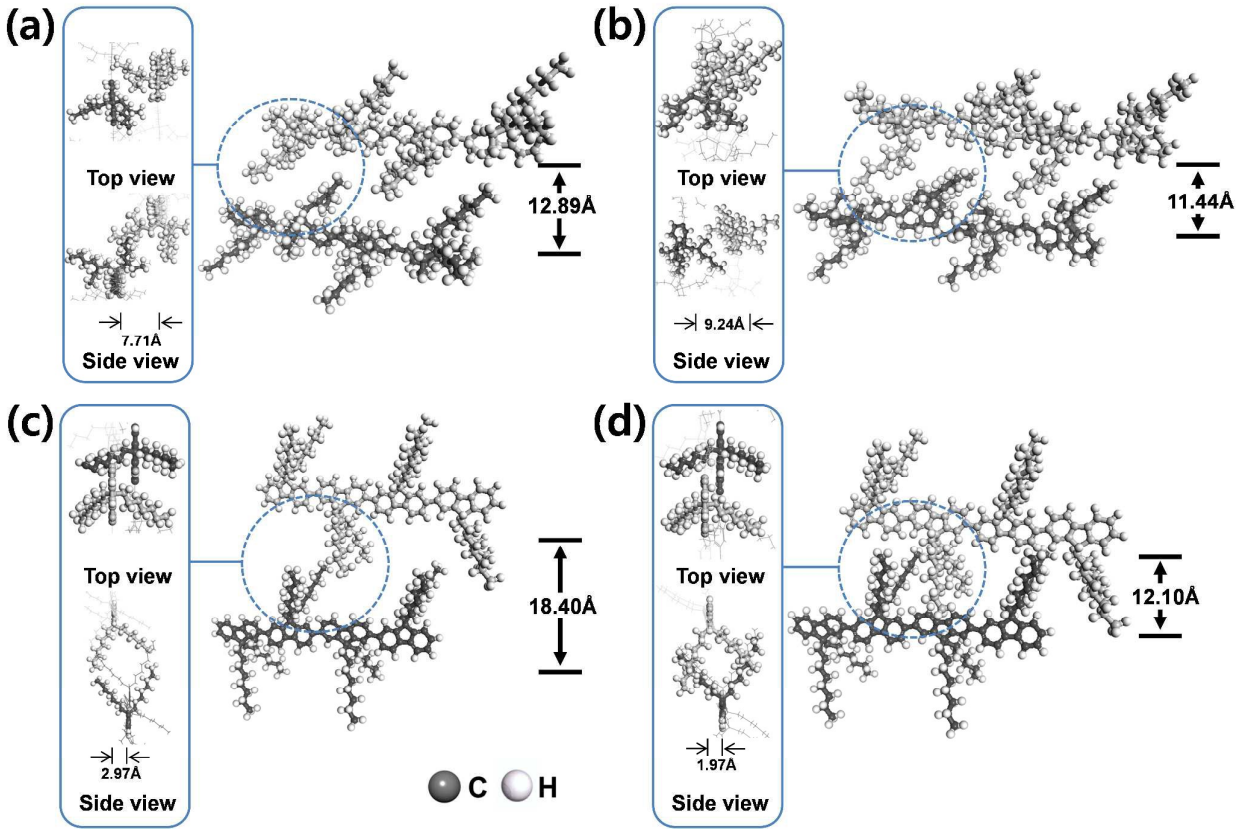

Fig. 5. Optimized geometry of two layers of (a) non-interdigitated PF2/6, (b) interdigitated PF2/6, (c) non-interdigitated PF8, and (d) interdigitated PF8.

In Fig. 5b, PF2/6 also showed considerable disorder (i.e., the backbone structure was distorted with a loss of side chain order),[47] which suggests that the interdigitation of PF2/6 is unfavorable. In particular, when the geometry of PF2/6 turns from non-interdigitated (5a) into interdigitated (5b), the disorder of the side chain geometry in PF2/6 causes repulsion between the layers, increasing the ring-plane distance from 7.71 to 9.24 Å. Although the interlayer distance for both the PFs was not exactly same with the experimental results (Table S1), the side chain molecules in PF2/6 unlikely fill the side chain region if it has the interdigitation conformation, according to the results form DFT and side chain packing model. It is assumed that the driving force form the molecular orientation at the film top surface could not exceed the opposite force of the adjacent molecule that has an intermediately rigid backbone at the nematic melt state. In contrast, the order of the side chains in PF8 was maintained with a stable geometry. The favorable side chain structure for interdigitation led to a change in molecular configuration of the neighboring molecules, which rendered PF8 more thermochromic than PF2/6. This kind of reorientation caused by a minor seed layer after entering the nematic melt state resembles the reorientation behavior of poly(2,5-bis(3-alkylthiophen-2-yl)thieno[3,2-b]thiophene) (pBTTT).[47-49] For both the cases of PF8 and pBTTT, transferring the orientation through side chains would also be a driving force to align. Therefore, we suggest that 3D intermolecular registry depends on both the side chain interdigitation and the π-orbital interactions between conjugated ring planes.[5,39,50]

Conclusions

We have shown that a previously unreported self-alignment of PF8 can be achieved after annealing in its nematic melt state. Direct rubbing of the surface can orient polymer segments in the top-most region of the film. Notably, in PF8, the orientation propagated much further into the bulk of the film. In PF2/6, which has side chains with a larger number of methylenes per volume than those in PF8, the rubbing-induced molecular orientation completely disappeared after entering the nematic phase because the disorder of the side chains in PF2/6 caused the oriented configuration to be lost. The integrated experimental studies and theoretical analysis indicated that the higher order of the side chains of PF8 compared with PF2/6 allowed favorable self-alignment of PF8 with affinitive interdigitation. The results provide a synthetic design rule for electroluminescent polymeric materials to develop display devices with better legibility, such as polarizer-free OLEDs or back light units in LCDs, without using alignment layers.

References

1 G. Yu, J. Gao, J. C. Hummelen, F. Wudl and A. J. Heeger, *Science*, 1995, **70**, 1789−1791.
2 G. Horowitz, *J. Mater. Res*., 2004, **19**, 1946−1962.
3 J. H. Burroughes, D. D. C. Bradley, A. R. Brown, R. N. Marks, K. Mackay, R. H. Friend, P. L. Burns and A. B. Holmes, *Nature*, 1990, **347**, 539−541.
4 M. Grell, D. D. C. Bradley, M. Inbasekaran and E. P. Woo, *Adv. Mater.*, 1997, **9**, 798−802.
5 R. J. Kline, D. M. DeLongchamp, D. A. Fischer, E. K. Lin, L. J. Richter, M. Chabinyc, M. Toney, M. Heeney and I. McCulloch, *Macromolecules*, 2007, **40**, 7960−7965.
6 D. M. DeLongchamp, R. J. Kline, E. K. Lin, D. A. Fischer, L. J. Richter, L. A. Lucas, M. Heeney, I. McCulloch and J. E. Northrup, *Adv. Mater*., 2007, **19**, 833−837.
7 I. McCulloch, M. Heeney, C. Bailey, K. Genevicius, I. Macdonald, M. Shkunov, D. Sparrowe, S. Tierney, R. Wagner, W. M. Zhang, M. Chabinyc, R. J. Kline, M. D. McGehee and M. F. Toney, *Nat. Mater*., 2006, **5**, 328−333.
8 M. Redecker, D. D. C. Bradley, M. Inbasekaran and E. P. Woo, *Appl. Phys. Lett*., 1999, **74**, 1400−1402.
9 M. Fukuda, K. Sawada and K. Yoshino, *Jpn. J. Appl. Phys*., 1989, **28**, L1433−L1435.
10 Y. Yang and Q. Pei, *J. Am. Chem. Soc*., 1996, **118**, 7416−7417.
11 M. Grell, W. Knoll, D. Lupo, A. Meisel, T. Miteva, D. Neher, H. G. Nothofer, U. Scherf and A. Yasuda, *Adv. Mater*., 1999, **11**, 671−675.
12 M. Kreyenschmidt, G. Klaerner, T. Fuhrer, J. Ashenhurst, S. Karg, W. D. Chen, V. Y. Lee, J. C. Scott and R. D. Miller, *Macromolecules*., 1998, **31**, 1099−1103.
13 B. Zhang, C. Qin, J. Ding, L. Chen, Z. Xie, Y. Cheng and L. Wang, *Adv. Funct. Mater*., 2010, **20**, 2951−2957.
14 A. Hasan, M. O. Sandberg, O. Nur and M. Willander, *Adv. Opt. Mater.*, 2014, **2**, 326−330.
15 Y. Yang and Q. Pei, *J. Appl. Phys*., 1997, **81**, 3294−3298.
16 Y. Y. Deng and H. Sirringhaus, *Phys. Rev. B*, 2005, **72**, 045207/1−12.
17 L. L. Lavery, G. L. Whiting and A. C. Arias, *Org. Electron*., 2011, **12**, 682−685.
18 B. Schartel, V. Wachtendorf, M. Grell, D. D. C. Bradley and M. Hennecke, *Phys. Rev. B*, 1999, **60**, 277−283.
19 B. Minaev, G. Baryshnikov and H. Agren, *Phys. Chem. Chem. Phys.*, 2014, **16**, 1719-1758.
20 D. Neher, *Macromol. Rapid Commun*., 2001, **22**, 1365−1385.
21 U. Scherf and E. J. W. List, *Adv. Mater*., 2002, **14**, 477−487.
22 K. Sakamoto, K. Usami, Y. Uehara and S. Ushioda, *Appl. Phys. Lett.*, 2005, **87**, 211910/1−3.
23 J.-W. Chen, C.-C. Huang and C.-Y. Chao, *ACS Appl. Mater. Interfaces.*, 2014, **6**, 6757−6764.
24 J. Teetsov and M. A. Fox, *J. Mater. Chem.*, 1999, **9**, 2117−2122.
25 M. Grell, D. D. C. Bradley, G. Ungar, J. Hill and K. S. Whitehead, *Macromolecules*, 1999, **32**, 5810−5817.
26 G. Lieser, M. Oda, T. Miteva, A. Meisel, H. G. Nothofer, U. Scherf and D. Neher, *Macromolecules*, 2000, **33**, 4490−4495.
27 S.-F. Chung, T.-C. Wen, Y.-W. Chou and T.-F. Guo, *Jpn. J. Appl. Phys.*, 2006, **45**, L60−L63.
28 M. Nishikawa, B. Taheri and J. L. West, *Appl. Phys. Lett*., 1998, **72**, 2403−2405.
29 D. D. C. Bradley, *J. Phys. D: Appl. Phys*., 1987, **20**, 1389−1410.
30 L. Biniek, N. Leclerc, T. Heiser, R. Bechara and M. Brinkmann, *Macromolecules*, 2013, **46**, 4014−4023.
31 Y. Liu, T. P. Russell, M. G. Samant, J. Stohr, H. R. Brown, A. Cossy-Favre and J. Diaz, *Macromolecules*, 1997, **30**, 7768−7771.
32 Y. Jung, T. Cho, D. Y. Yoon, C. W. Frank and J. Luning, *Macromolecules*, 2005, **38**, 867−872.
33 T. Yamamoto, D. Komarudin, M. Arai, B. L. Lee, H. Suganuma, N. Asakawa, Y. Inoue, K. Kubota, S. Sasaki, T. Fukuda and H. Matsuda, *J. Am. Chem. Soc*., 1998, **120**, 2047−2058.
34 A. Sakko, M. Hakala, J. A. Soininen and K. Hämäläinen, *Phys. Rev. B,* 2007, **76**, 205115/1−7.
35 J. E. Northrup, *Phys. Rev. B*, 2007, **76**, 245202/1−6.
36 J. Jo, C. Chi, S. Höger, G. Wegner and D. Y. Yoon, *Chem. Eur. J*. 2004, **10**, 2681−2688.
37 Materials studio v8. Accelrys, Inc., San Diego 2015.
38 J. P. Perdew, K. Burke and M. Ernzerhof, *Phys. Rev. Lett*., 1996, **77**, 3865−3868.
39 H. Kikuchi, J. A. Logan and D. Y. Yoon, *J. Appl. Phys*., 1996, **79**, 6811−6817.
40 J. C. Love, L. A. Estroff, J. K. Kriebel, R. G. Nuzzo and G. M. Whitesides, *Chem. Rev*., 2005, **105**, 1103−1169.
41 G. L. Gibson, D. Gao, A. A. Jahnke, J. Sun, A. J. Tilley and D. D. Seferos, *J. Mater. Chem. A*, 2014, **2**, 14468−14480.
42 M. Knaapila, Z. Konôpková, M. Torkkeli, D. Haase, H.-P. Liermann, S. Guha and U. Scherf, *Phys. Rev. E*, 2013, **87**, 022602.
43 Y. Nakano, Y. Liub and M. Fujiki, *Polym. Chem*., 2010, **1**, 460−469.
44 M. Knaapila, R. Stepanyan, B. P. Lyons, M. Torkkeli and A. P. Monkman, *Adv. Funct. Mater*., 2006, **16**, 599−609.
45 S.-H. Chen, A. C. Su, C. H. Su and S. A. Chen, *Macromolecules*, 2005, **38**, 379−385.
46 A. Bolognesi, F. Galeotti, J. Moreau, U. Giovanella, W. Porzio, G. Scaviaab and F. Bertiniab, *J. Mater. Chem*., 2010, **20**, 1483−1488.
47 S. Himmelberger, D. T. Duong, J. E. Northrup, J. Rivnay, F. P. V. Koch, B. S. Beckingham, N. Stingelin, R. A. Segalman, S. C. B. Mannsfeld and A. Salleo, *Adv. Funct. Mater*., 2015, **25**, 2616−2624.
48 D. M. DeLongchamp, R. J. Kline, Y. Jung, D. S. Germack, E. K. Lin, A. J. Moad, L. J. Richter, M. F. Toney, M. Heeney and I. McCulloch, *ACS Nano*, 2009, **3**, 780−787.
49 M. J. Lee, D. Gupta, N. Zhao, M. Heeney, I. McCulloch and H. Sirringhaus, *Adv. Funct. Mater*., 2011, **21**, 932–940.
50 S. W. Lee, B. Chae, H. C. Kim, B. Lee, W. Choi, S. B. Kim, T. Chang and M. Ree, *Langmuir*, 2003, **19**, 8735−8743.

Graphical abstract

Title: Influence of Side Chains on the Self-alignment Capability of Electroluminescent Polyfluorenes

Y. Jung,* S. Kwon,* S. Lee, Y. Yang

Side chain structure gives critical role in the orientation propagation of an aligned seed layer into the bulk of the polyfluorene film by heating into its nematic melt state.